

Quantum criticality among entangled spin chains

N. Blanc¹, J. Trinh¹, L. Dong^{2,3}, X. Bai⁴, A. A. Aczel⁵, M. Mourigal⁶, L. Balents⁶, T. Siegrist^{2,3}
and A. P. Ramirez^{1*}

An important challenge in magnetism is the unambiguous identification of a quantum spin liquid^{1,2}, of potential importance for quantum computing. In such a material, the magnetic spins should be fluctuating in the quantum regime, instead of frozen in a classical long-range-ordered state. While this requirement dictates systems^{3,4} wherein classical order is suppressed by a frustrating lattice⁵, an ideal system would allow tuning of quantum fluctuations by an external parameter. Conventional three-dimensional antiferromagnets can be tuned through a quantum critical point—a region of highly fluctuating spins—by an applied magnetic field. Such systems suffer from a weak specific-heat peak at the quantum critical point, with little entropy available for quantum fluctuations⁶. Here we study a different type of antiferromagnet, comprised of weakly coupled antiferromagnetic spin-1/2 chains as realized in the molecular salt $K_2PbCu(NO_2)_6$. Across the temperature-magnetic field boundary between three-dimensional order and the paramagnetic phase, the specific heat exhibits a large peak whose magnitude approaches a value suggestive of the spinon Sommerfeld coefficient of isolated quantum spin chains. These results demonstrate an alternative approach for producing quantum matter via a magnetic-field-induced shift of entropy from one-dimensional short-range order to a three-dimensional quantum critical point.

Previous work on field-tuning of quantum fluctuations has focused on the transverse-field Ising model where the magnetic field (H) couples to a sector of the Hamiltonian not directly modifying the order parameter. While this paradigm has been explored in the three-dimensional (3D) dipolar ferromagnet $LiHoF_4$ (refs 7,8), and the 1D system $CoNb_2O_6$ (ref. 9), the need for a unique Ising-axis normal restricts the number of potential quantum-spin-liquid host materials. For the much broader class of 3D antiferromagnets (AFs), H can indeed tune the Néel temperature (T_N) into the quantum regime. Within the ordered state, however, on increasing H from zero one first encounters a spin-flop transition (for finite spin anisotropy), followed by a gradual reorientation of those spins (Fig. 1a). Hence, in destroying Néel order, H decreases the transverse components of the staggered moment to a value that is vanishingly small near the transition to the field-polarized state, leaving little entropy to be lost near $T=0$, and thus low spectral weight available for quantum entanglement⁶.

Here we demonstrate a different approach to tuning through a quantum critical point (QCP). The quasi-1D spin-1/2 AF $K_2PbCu(NO_2)_6$ orders classically at 0.68 K (ref. 10; Fig. 1b). At lower temperatures within the Néel state, applied H values less than the intra-chain mean field cause little change in the specific heat $C(T, H)$. At the phase boundary, however, a large amount of entropy is released, leading to a peak in C/T (Fig. 1c), the value of which ($\sim 2J \text{ mol}^{-1} \text{ K}^{-2}$ at the lowest

temperatures studied) is suggestive of the spinon Sommerfeld coefficient observed in uncoupled Heisenberg spin-1/2 chains¹¹. This competition between H and singlet-like short-range order is reminiscent of spin-dimer QCPs^{12,13} and suggests a much larger family of materials for creating highly fluctuating quantum matter.

We grew single crystals of $K_2PbCu(NO_2)_6$ using a custom gel-growth technique¹⁴ (see Methods). At $T=280 \text{ K}$, $K_2PbCu(NO_2)_6$ (elpasolite structure denoted CuElp, face-centred-cubic lattice, space group $Fm\bar{3}$) undergoes a Jahn–Teller distortion^{15,16}. This distortion leads to an antiferro-distortive pattern of elongation axes¹⁵ of the Cu–NO₂ octahedra in the a – b plane, and a 2% contraction along the c axis (see Fig. 1c inset). This contraction is responsible for quasi-1D behaviour as evidenced by a good fit of the magnetic susceptibility, $\chi(T)$, to the Bonner–Fisher result for isolated 1D spin chains with Hamiltonian $H = \sum J S_i \cdot S_j$ (ref. 17), yielding an intra-chain exchange energy $J/k_B = 5.4 \text{ K}$ (Fig. 2a). Isomorphic $Rb_2PbCu(NO_2)_6$ displays similar behaviour¹⁸. In $K_2PbCu(NO_2)_6$, we find a saturation field of $H_s \sim 7 \text{ T}$ at $T = 1.7 \text{ K}$ (Fig. 2b); thus, the collective behaviour in CuElp is tunable with modest magnetic fields.

Previous $C(T, H=0)$ measurements on $K_2PbCu(NO_2)_6$ show a single broad λ peak, signalling a transition to 3D order around $T_N \sim 0.50 \text{ K}$ (ref. 19). Our elastic neutron scattering measurements down to $T=0.3 \text{ K}$ at $H=0$ (Fig. 2c,d,f) and $C(T, H)$ measurements up to $H=6 \text{ T}$ (Figs. 1 and 2e) confirm that this transition is to an AF state. In Fig. 1c, $C(T)$ for CuElp is shown in fixed fields. At $H=0$, three peaks are evident, a result reproduced in four different crystals synthesized in three different growth runs. The highest temperature peak at $T_h = 0.68 \text{ K}$ corresponds to the temperature at which magnetic Bragg scattering (Fig. 2c,d) is first seen on cooling (Fig. 2f). A second peak is seen at $T_m = 0.58 \text{ K}$ and a third at $T_l = 0.51 \text{ K}$. At $H=1 \text{ T}$, the peak at T_l sharpens and is visible up to 2 T, but has vanished by 3 T. The termination of this T_l line implies it is not symmetry-lowering, and possibly a spin-flop transition. The other two transitions are robust along the entire phase boundary. The low-field nature of this boundary is of interest. While T_N decreases with increasing H in the mean-field approximation, more accurate techniques reveal small positive $\partial T_N / \partial H$ values due to spin dimensionality reduction¹⁹, which is pronounced for quasi-1D systems²⁰. Comparing $\partial T_N / \partial H$ of CuElp in reduced units with other 1D magnets, we find that the behaviour is similar to that seen in $(NC_5H_6)_2MnCl_3 \cdot H_2O$ for which $J/J_i = 14$ (ref. 20), where J_i is the effective inter-chain coupling (in CuElp, this would be derived from J' , J'' and J shown in Fig. 1c inset). Determination of J_i will require inelastic neutron scattering, planned for future work.

Our elastic neutron scattering experiment at $H=0$ is sensitive to static magnetic correlations contained within the (hhl) plane, where h and l span the reciprocal lattice of the room-temperature cubic unit cell. At $T=0.29 \text{ K}$, we observe a Bragg peak at wavevector $\mathbf{q}=(0,0,1/2)$

¹UC Santa Cruz, Santa Cruz, CA 95064, USA. ²FAMU-FSU College of Engineering, Tallahassee, FL 32310, USA. ³National High Magnetic Field Laboratory, Tallahassee, FL 32310, USA. ⁴School of Physics, Georgia Institute of Technology, Atlanta, GA 30332, USA. ⁵Neutron Scattering Division, Oak Ridge National Laboratory, Oak Ridge, TN 37831, USA. ⁶Kavli Institute for Theoretical Physics, UC Santa Barbara, Santa Barbara, CA 93106, USA. N. Blanc and J. Trinh contributed equally to this work. *e-mail: apram@ucsc.edu

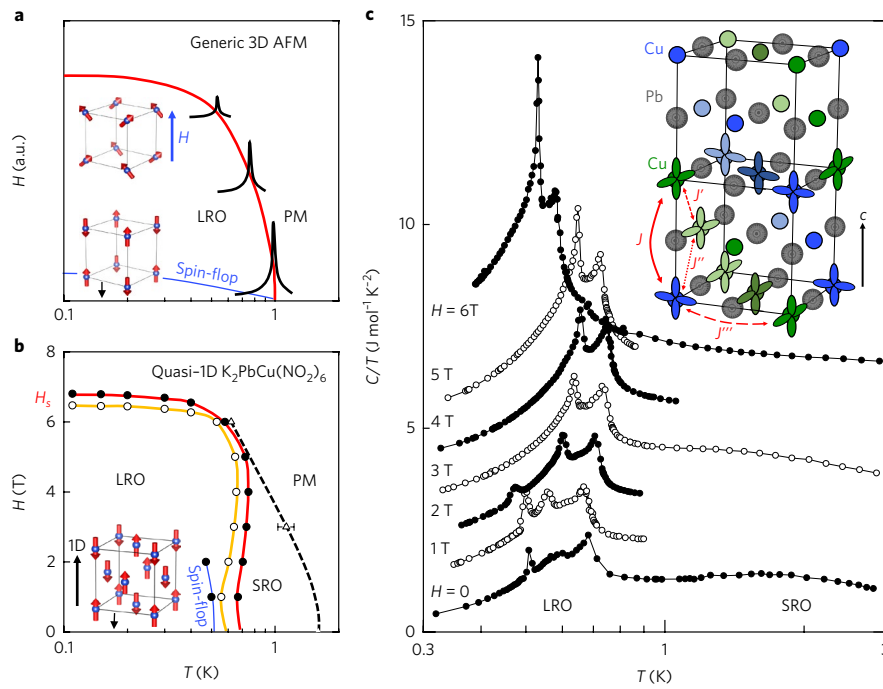


Fig. 1 | Comparison of the T - H phase diagram for the quasi-1D system $\text{K}_2\text{PbCu}(\text{NO}_2)_6$ with the behaviour of a generic 3D antiferromagnet. **a, Sketch of the phase diagram of a conventional 3D antiferromagnet showing the AF phase, the spin-flop phase and the expected $C(T)$ on the phase boundary. LRO, long-range order; PM, paramagnetic. **b**, T - H phase diagram of $\text{K}_2\text{PbCu}(\text{NO}_2)_6$ showing a possible ordered state consistent with neutron scattering. SRO, short-range order. **c**, Specific heat divided by temperature versus temperature for $\text{K}_2\text{PbCu}(\text{NO}_2)_6$. Each curve is offset vertically by H in tesla times $1 \text{ J mol}^{-1} \text{ K}^{-2}$ (inset). Crystal structure of $\text{K}_2\text{PbCu}(\text{NO}_2)_6$ showing the Cu and Pb atoms, with K and NO_2 omitted¹⁸. The Jahn-Teller-induced orbital order is depicted for some of the Cu atoms as e_g -like lobes. Here, J is the dominant intra-chain interaction, with J' , J'' and J''' responsible for inter-chain interactions.**

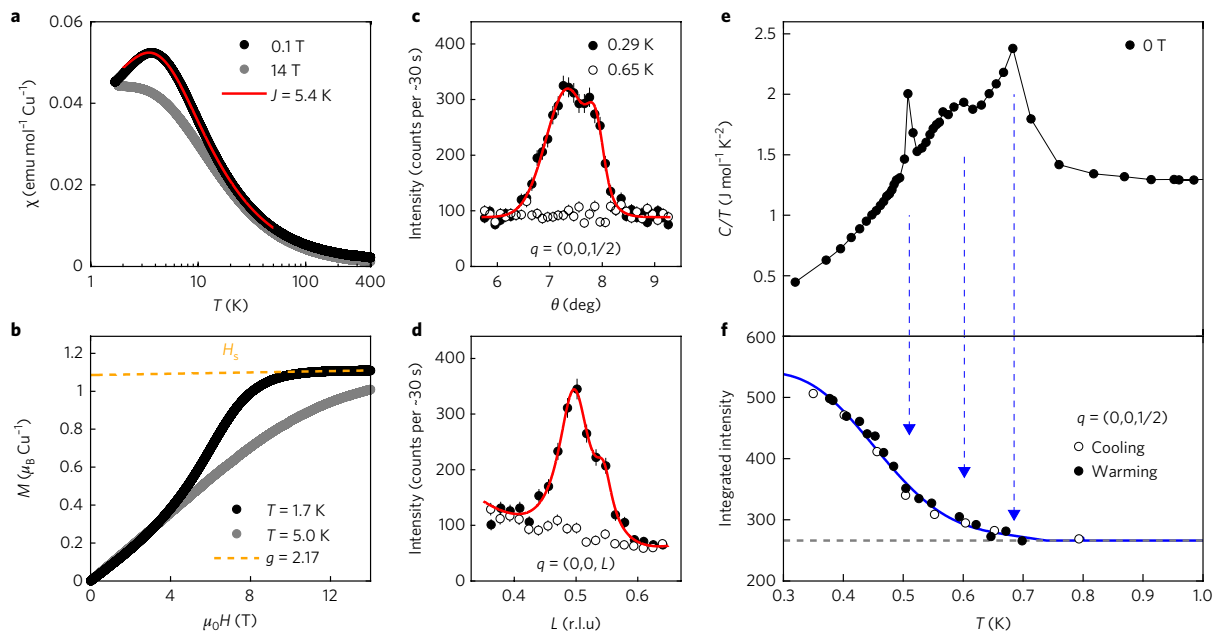


Fig. 2 | Magnetic properties of $\text{K}_2\text{PbCu}(\text{NO}_2)_6$ showing quasi-1D behaviour and antiferromagnetic order. **a, Temperature dependence of the magnetic susceptibility in a field of 0.1 T (black symbols) and 14 T (grey symbols). The solid red line is a fit to the data with the Bonner-Fisher susceptibility in the temperature range from 2 K to 50 K with $J = 5.4 \text{ K}$. **b**, Isothermal magnetization at temperatures of 1.7 K (black symbols) and 5 K (grey symbols). The dashed red line is a fit to the field-linear part of the magnetization above 12 T and yields a saturated magnetization M_s of $1.08\mu_B$. **c**, Rocking curve around the $(0,0,1/2)$ position of the cubic unit cell obtained by elastic neutron scattering at 0.29 K (filled symbols) and 0.65 K (open symbols). A fit with a double Gaussian profile is indicated by the red line. **d**, Longitudinal scan at the $(0,0,1/2)$ position at the same temperatures. A fit with a double Lorentzian profile is indicated by the red line. **e**, Low-temperature part of the magnetic specific heat divided by temperature in zero magnetic field. **f**, Integrated neutron scattering intensity at the $(0,0,1/2)$ Bragg peak position as a function of temperature and cooling protocol. The blue line is a guide to the eye. Dashed vertical arrows indicate the correspondence between features in the magnetic heat capacity and changes in the temperature slope of the integrated neutron scattering intensity.**

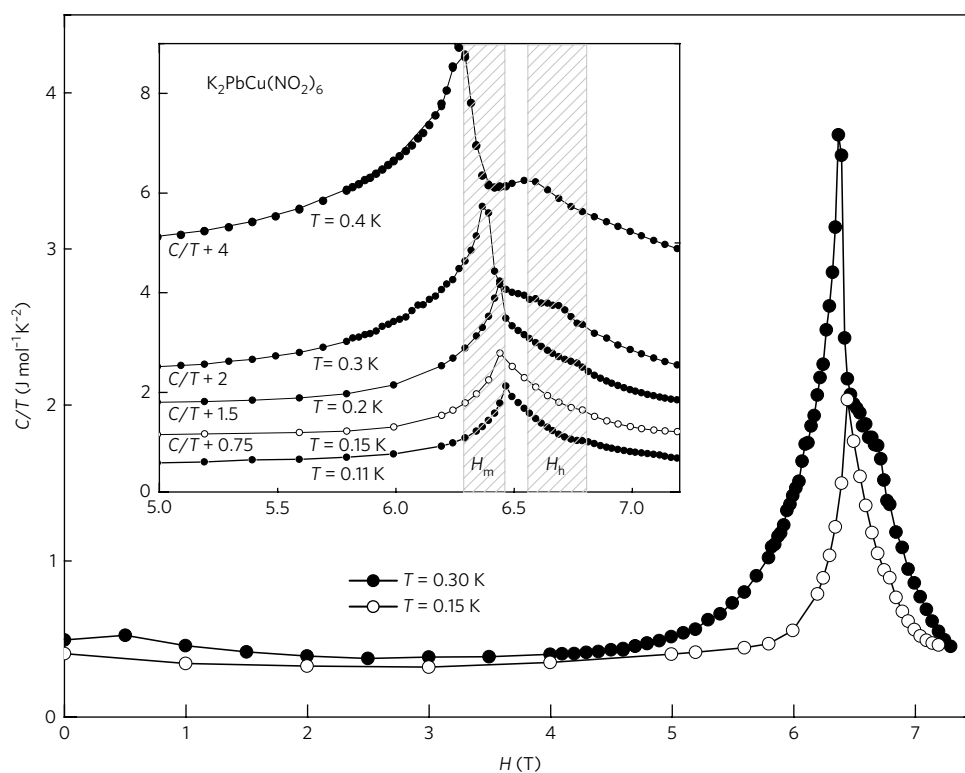


Fig. 3 | Specific heat divided by temperature, $C(T,H)/T$, versus magnetic field for $\text{K}_2\text{PbCu}(\text{NO}_2)_6$. The main frame shows the behaviour over a wide H range. Inset: $C(T,H)/T$ versus field near the QCP at five different temperatures. The curves have been offset by an amount in $\text{J mol}^{-1} \text{K}^{-2}$ as indicated. The shaded regions correspond to the regions of change for the critical fields H_m and H_h .

(Fig. 2c,d), which vanishes above $T=0.65\text{ K}$, consistent with the $C(T)$ anomalies (Fig. 2e). The peak shoulder at $l \approx 0.53$ r.l.u. (Fig. 2d) reflects the 1.2° full-width at half-maximum rocking curve (Fig. 2c) of Bragg peaks broadened by the Jahn–Teller distortion. Our survey of the (hhl) plane identifies more than ten other Bragg reflections all indexed by $\mathbf{q} = \tau \pm \mathbf{k}_m$, where τ is a reciprocal lattice vector and $\mathbf{k}_m = (0,0,1/2)$ is the magnetic propagation vector. A candidate magnetic structure at $T=0.3\text{ K}$ is shown in Fig. 1b (inset). The temperature dependence of the magnetic signal, obtained by integrating the $\mathbf{q} = (0,0,1/2)$ Bragg intensity is shown in Fig. 2f. No difference is found between warming or cooling, demonstrating good sample thermalization. The integrated intensity changes non-trivially with temperature, presumably reflecting the three peaks in $C(T)$.

In Fig. 3 we show $C(T,H)$ at different fixed temperatures as a function of H from 0 to 7.2 T. The first striking aspect of these data is the weak H dependence over most of the range. Within the Néel state of a system with isotropic interactions and weak single-ion anisotropy, the continuous spin rotation induced by an increasing H leads to a broad peak in $C(T,H)$ with a maximum at roughly half the critical field, H_c , as seen in Yb_3Pt_4 (ref. 6). The second striking aspect of our data is a sharp peak in $C(T,H)$ at a value, H_m , consistent with the phase formed at T_m in the T -dependent sweeps in Fig. 1c. (At an H value $\sim 5\%$ larger than H_m , a second, smaller peak at H_h is seen, identifiable with the fixed-field T_h .) Such a large anomaly has not been observed in the response of an AF to a longitudinal field, although recent measurements in diluted $\text{CePd}_{0.95}\text{Ni}_{0.05}\text{Al}$ bear some similarity to our results²¹. We also note the disparity between the magnitudes of T_N and H_m . In 3D AFs, $k_B T_N \sim g\mu_B H_c$, where $g=2$. For CuElp , by identifying H_m with H_c , we find $k_B T_N \sim 0.075 g\mu_B H_c$, implying that the ordering degrees of freedom are not individual spins, but entities that approximate singlets, consistent with ordering among spin chains.

The collective behaviour within isolated $S=1/2$ Heisenberg chains is well understood through exact results (Bethe ansatz) and

low-energy effective field theory²². The full form of $C(T,H)$ is exactly known²³ and yields a Sommerfeld form $C(T,H) = \gamma(H)T$, where $\gamma(H) = \pi R / (3v_s(H)/k_B)$, R is the gas constant and $v_s(H)$ is the field-dependent spinon velocity. Experimentally, such a linear-in- T term at $H=0$ was found in $\text{Cu}(\text{pyrazine})(\text{NO}_2)_2$ (CuPzN)²⁴ and copper benzoate²⁵. For finite H , the thermodynamic Bethe ansatz was applied and confirmed experimentally in CuPzN (ref. 11) for fields well below H_s , the predicted magnetization saturation field¹¹. Figure 4 shows the heights of the measured peaks in comparison with the spinon γ calculated for two different H values. The seemingly asymptotic behaviour of $C(T,H)$ at values close to that predicted for isolated chains suggests the importance of 1D character for the present QCP. Regarding the functional form of $C(T,H)$ for isolated chains, the point $T=0, H=H_s$ is a 1 + 1D quantum phase transition, and near H_s takes on a quantum critical form, with $C(H,T)/T = T^{-1/2}F((H-H_s)/T)$, where $F(h)$ is a universal function (see Supplementary Information). Remarkably, this QCP is described by free fermions, from which we obtain $F(h)$. We find that it—and hence $C(H)/T$ —demonstrates a two-peak behaviour, shown in the inset of Fig. 4. While the measured $C(H)/T$ is qualitatively similar to this theoretical result, important differences exist between them. First, the experimental peak in $C(H)/T$ decreases with decreasing temperature, seemingly approaching a fixed value close to that found in the Bethe ansatz calculation. Second, the experimental peak separation in H does not vary linearly with field in the same range of reduced temperature. It is important to note, however, that the calculation is performed for a single chain, whereas, experimentally, the chains are coupled, and indeed three-dimensionally ordered, over most of the measurement range. While it is not feasible that the peak itself is caused by a nuclear Schottky or hyperfine contribution, the precise value of C/T might be influenced by such a contribution (see Methods). To accurately compare the measured C_{max}/T with single-chain theory, the mean field from the neighbouring chains must be accounted for. A full theoretical treatment of the

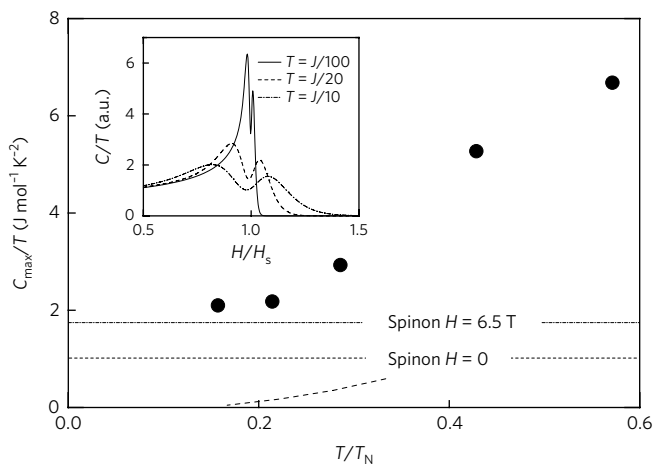


Fig. 4 | The temperature dependence of $C/T(H)$ peaks suggests an explanation based on spinons in 1D. The main frame shows the value of the peaks for the isotherms in Fig. 3, versus reduced temperature T/T_N . The dashed lines are Bethe ansatz values for the spinon Sommerfeld coefficient, calculated at both $H=0$ and close to the critical field, $H=6.5$ T. The solid line represents the C/T peak heights for the 3D spin-1/2 AF Yb_3Pt_4 . Adapted from ref. ⁶, APS. Inset: theoretical $C/T(H)$ of an AF Heisenberg chain for three different temperatures relative to the exchange coupling, J , in the chain. The lower temperature bound of our measurements is $J/20$.

problem would invoke chain mean-field theory of the 3D coupling, known to be accurate for several systems^{26–28}. In chain mean-field theory, intra-chain interactions are treated exactly while inter-chain interactions are handled within mean-field theory.

The key finding of this work is that the physics near a QCP is tunable with field, invoking a comparison to the dimer magnets TiCuCl_3 (ref. ¹²) and $\text{BaCuSi}_2\text{O}_6$ (ref. ²⁹). In contrast to the dimer systems, however, CuElp is ordered at fields below the QCP, not above. More generally, the above results point to an alternative approach towards realizing strongly fluctuating quantum criticality in magnets, namely using the competition between a large lower-dimensional (here 1D) two-spin antiferromagnetic interaction and magnetic field in tuning out of a 3D ordered state.

Methods

Methods, including statements of data availability and any associated accession codes and references, are available at <https://doi.org/10.1038/s41567-017-0010-y>.

Received: 21 March 2017; Accepted: 19 October 2017;
Published online: 11 December 2017

References

- Nayak, C., Simon, S. H., Stern, A., Freedman, M. & Das Sarma, S. Non-Abelian anyons and topological quantum computation. *Rev. Mod. Phys.* **80**, 1083–1159 (2008).
- Kitaev, A. Anyons in an exactly solved model and beyond. *Ann. Phys.* **321**, 2–111 (2006).
- Helton, J. S. et al. Spin dynamics of the spin-1/2 Kagome lattice antiferromagnet $\text{ZnCu}_3(\text{OH})_6\text{Cl}_2$. *Phys. Rev. Lett.* **98**, 107204 (2007).
- Yamashita, M. et al. Thermal-transport measurements in a quantum spin-liquid state of the frustrated triangular magnet kappa-(BEDT-TTF)₂Cu₂(CN)₃. *Nat. Phys.* **5**, 44–47 (2009).
- Ramirez, A. P. Strongly geometrically frustrated magnets. *Annu. Rev. Mater. Sci.* **24**, 453–480 (1994).
- Wu, L. S. et al. Magnetic field tuning of antiferromagnetic Yb_3Pt_4 . *Phys. Rev. B* **84**, 134409 (2011).
- Bitko, D., Rosenbaum, T. F. & Aeppli, G. Quantum critical behavior for a model magnet. *Phys. Rev. Lett.* **77**, 940–943 (1996).

8. Ghosh, S., Rosenbaum, T. F., Aeppli, G. & Coppersmith, S. N. Entangled quantum state of magnetic dipoles. *Nature* **425**, 48–51 (2003).
9. Coldea, R. et al. Quantum criticality in an Ising chain: experimental evidence for emergent E-8 symmetry. *Science* **327**, 177–180 (2010).
10. Blote, H. W. J. Magnetically linear and quadratic hexanitocuprates. *J. Appl. Phys.* **50**, 1825–1827 (1979).
11. Hammar, P. R. et al. Characterization of a quasi-one-dimensional spin-1/2 magnet which is gapless and paramagnetic for $g\mu_B H$ less than or similar to J and $k_B T \ll J$. *Phys. Rev. B* **59**, 1008–1015 (1999).
12. Nikuni, T., Oshikawa, M., Oosawa, A. & Tanaka, H. Bose-Einstein condensation of dilute magnons in TiCuCl_3 . *Phys. Rev. Lett.* **84**, 5868–5871 (2000).
13. Jaime, M. et al. Magnetic-field-induced condensation of triplons in Han purple pigment $\text{BaCuSi}_2\text{O}_6$. *Phys. Rev. Lett.* **93**, 087203 (2014).
14. Dong, L., Besara, T., Henderson, A. & Siegrist, T. Gel growth of $\text{K}_2\text{PbCu}(\text{NO}_2)_6$ -elpasolite single crystals. *Cryst. Growth Des.* **17**, 5170–5177 (2017).
15. Noda, Y., Mori, M. & Yamada, Y. Successive Jahn–Teller phase-transitions in $\text{K}_2\text{PbCu}(\text{NO}_2)_6$. *J. Phys. Soc. Jpn* **45**, 954–966 (1978).
16. McConnell, J. D. C. & Heine, V. Origin of incommensurate structure in the cooperative Jahn–Teller system $\text{K}_2\text{PbCu}(\text{NO}_2)_6$. *J. Phys. C* **15**, 2387–2402 (1982).
17. Bonner, J. C. & Fisher, M. E. Linear magnetic chains with anisotropic coupling. *Phys. Rev.* **135**, A640–A658 (1964).
18. Okuda, K., Mollmotto, H., Miyako, Y., Mori, M. & Date, M. One-dimensional antiferromagnetism in $\text{Rb}_2\text{PbCu}(\text{NO}_2)_6$. *J. Phys. Soc. Jpn* **53**, 3616–3623 (1984).
19. Kosterlitz, J. M., Nelson, D. R. & Fisher, M. E. Bicritical and tetracritical points in anisotropic antiferromagnetic systems. *Phys. Rev. B* **13**, 412–432 (1976).
20. Hijmans, J., Kopinga, K., Boersma, F. & Dejonge, W. J. M. Phase-diagrams of pseudo one-dimensional Heisenberg systems. *Phys. Rev. Lett.* **40**, 1108–1111 (1978).
21. Sakai, A. et al. Signature of frustrated moments in quantum critical $\text{CePd}_{1-x}\text{Ni}_x\text{Al}$. *Phys. Rev. B* **94**, 220405 (2016).
22. Tsvetlik, A. M. *Quantum Field Theory in Condensed Matter Physics* (Cambridge Univ. Press, Cambridge, 1995).
23. Klumper, A. The spin-1/2 Heisenberg chain: thermodynamics, quantum criticality and spin-Peierls exponents. *Eur. Phys. J. B* **5**, 677–685 (1998).
24. Mennenga, G., Dejongh, L. J., Huiskamp, W. J. & Reedijk, J. Specific-heat and susceptibility of the 1-dimensional $S=1/2$ Heisenberg-antiferromagnet $\text{Cu}(\text{Pyrazine})(\text{NO}_2)_2$ - evidence for random exchange effects at low-temperatures. *J. Magn. Magn. Mater.* **44**, 89–98 (1984).
25. Dender, D. C., Hammar, P. R., Reich, D. H., Broholm, C. & Aeppli, G. Direct observation of field-induced incommensurate fluctuations in a one-dimensional $S=1/2$ antiferromagnet. *Phys. Rev. Lett.* **79**, 1750–1753 (1997).
26. Scalapino, D. J., Imry, Y. & Pincus, P. Generalized Ginzburg–Landau theory of pseudo-one-dimensional systems. *Phys. Rev. B* **11**, 2042–2048 (1975).
27. Sandvik, A. W. Multichain mean-field theory of quasi-one-dimensional quantum spin systems. *Phys. Rev. Lett.* **83**, 3069–3072 (1999).
28. Starykh, O. A., Katsura, H. & Balents, L. Extreme sensitivity of a frustrated quantum magnet: Cs_2CuCl_4 . *Phys. Rev. B* **82**, (2010)
29. Sebastian, S. E. et al. Dimensional reduction at a quantum critical point. *Nature* **441**, 617–620 (2006).

Acknowledgements

This work was supported by NSF-DMR 1534741 (A.P.R.), NSF-DMR1506119 (L.B.) and NSF-DMR 1534818 (T.S., L.D.). The research at Georgia Tech was supported by Oak Ridge Associated Universities through the Ralph E. Powe Junior Faculty Enhancement Award (M.M.). The research at Oak Ridge National Laboratory's High Flux Isotope Reactor was sponsored by the US Department of Energy, Office of Basic Energy Sciences, Scientific User Facilities Division. The research at the National High Magnetic Field Laboratory was supported by the NSF Collaborative Agreement DMR 1157490 and the State of Florida. We thank G. Aeppli, M. E. Fisher, D. Reich and C. M. Varma for their helpful insights.

Author contributions

A.P.R. designed the experiment, and with N.B. and J.T. collected and analysed specific-heat data. T.S. and L.D. grew crystals and analysed susceptibility data. X.B., A.A. and M.M. performed neutron scattering and magnetization measurements and analysed the data. L.B. provided theoretical interpretation of results.

Competing interests

The authors declare no competing financial interests.

Additional information

Supplementary information is available for this paper at <https://doi.org/10.1038/s41567-017-0010-y>.

Reprints and permissions information is available at www.nature.com/reprints.

Correspondence and requests for materials should be addressed to A.P.R.

Publisher's note: Springer Nature remains neutral with regard to jurisdictional claims in published maps and institutional affiliations.

Methods

Crystal preparation. Single crystals of $\text{K}_2\text{PbCu}(\text{NO}_2)_6$ (CuElp) were grown in potassium metasilicate gels with potassium nitrate, lead acetate and copper acetate as starting materials, by a method to be discussed separately¹⁴. In short, to achieve crystal sizes up to 50 mm^3 , the nucleation rate was reduced by limiting the reactant diffusion rate in the metasilicate gel, and allowing several weeks for room-temperature growth.

Magnetization and specific-heat measurements. Magnetization, and thus $\chi(T)$, was measured in a commercial superconducting quantum interference device magnetometer or using a vibrating sample magnetometer. The $C(T, H)$ data were obtained in a top-loading ^3He – ^4He dilution refrigerator using the semi-adiabatic heat-pulse method. The sapphire calorimeter used was tightly trussed by polyester threads anchored to the mixing chamber of the refrigerator with a force of approximately 0.5 N, which is 10^4 times the maximum H -induced rotational force on the sample given a similar 10% g -factor anisotropy as reported for the Rb compound¹⁸. The sample used for $C(T, H)$ had a cubic habit and was bonded via a (100) face to the calorimeter with silicone grease. To determine C as a smooth function of H at fixed T , data were taken in a narrow region encompassing the T value of interest for each field. The data were then fitted to a straight line, the H -dependent parameters of which allow the computation of $C(T)$ at an arbitrary T in the narrow range. Measurements were restricted to T values above 0.1 K, below which the onset of Kapitza thermal resistance and our sample size together make the temperature relaxation time to the bath greater than the internal relaxation time. Regarding sample orientation, because the Jahn–Teller distortion occurs from a cubic structure, the particular principal axis selected as the c axis on cooling could depend on aspects of the cooling procedure, the degree of mechanical clamping and the internal stresses in the crystal. For reasons to be discussed below, we believe that the $C(T, H)$ measurements reported here are on a sample cooled to achieve a single domain.

Regarding a possible nuclear contribution, the largest effect will most likely come from the Cu moments³⁰, and may become appreciable below 0.15 K. To accurately segregate the nuclear from the electronic contribution, however, it is necessary to enter a temperature regime where the $1/T^2$ nuclear Schottky tail can be cleanly distinguished. We found that below 0.10 K, however, the thermal time constant internal to the calorimeter became larger than the time constant to the bath, making the extraction of a nuclear contribution impossible. In addition,

it is not clear that the electronic contribution in the vicinity of the QCP will not also diverge, presenting an experimental challenge beyond the scope of the present work. For the present work, we note only that the high-temperature tail of a nuclear Schottky anomaly will vary as H^2 , which is not observed in our measurements.

Neutron scattering. Elastic neutron scattering was performed on the HB1A triple-axis spectrometer at the High Flux Isotope Reactor, Oak Ridge National Laboratory, USA. A 44 mg single crystal of $\text{K}_2\text{PbCu}(\text{NO}_2)_6$ was attached to an oxygen-free copper holder using copper wires and aligned at room temperature using a Multiwire X-ray Laue backscattering machine with the cubic directions [110] and [001] in the scattering plane. The mount was attached at the bottom of a ^3He insert reaching a base temperature of $T = 0.29 \text{ K}$. The wavelength of the incident neutron beam was set to 2.363 \AA using a double-bounce PG(002) monochromator and the scattered beam was analysed by PG(002) crystals. The beam was collimated to $40'$ (respectively, $270'$) before (respectively, after) the sample.

At room temperature, the strong (002), (220) and (004) nuclear Bragg reflections of our crystal are resolution limited with rocking curves showing full-width at half-maximum of 0.38° or lower. At $T_{s1} = 279 \text{ K}$ and $T_{s2} = 273 \text{ K}$, the compound exhibits the expected Jahn–Teller transitions¹⁵. For $T > T_{s1}$, the crystal structure is cubic (space group $Fm\bar{3}$, $a = 10.692 \text{ \AA}$), whereas below $T < T_{s2}$, the crystal structure is triclinic (space group $C-1$). Below T_{s2} , it remains possible to index nuclear Bragg reflections with respect to the reciprocal lattice vectors of the cubic structure $\tau = (h, k, l)_c$ with additional super-lattice reflections at $\mathbf{q} = \tau \pm \mathbf{k}_s$ with $\mathbf{k}_s = (1/2, 1/2, 1/2)_c$. In our experiment, the cubic-to-triclinic distortion is readily apparent on nuclear Bragg reflections (220)_c and (002)_c as pronounced non-Gaussian peak shapes, leading to an effective rocking-curve full-width at half-maximum ranging from 1.0° to 1.2° below T_{s2} .

Data availability. The data that support the findings of this study are available from the corresponding author upon reasonable request.

References

30. Heath, R. in *CRC Handbook of Chemistry and Physics* (ed. Weast, R.) (CRC Press, Boca Raton, FL, 1988).